Atmospheric Environment 45 (2011) 4213–4219

Contents lists available at ScienceDirect

Atmospheric Environment

journal homepage: www.elsevier.com/locate/atmosenv

Comparison between knife-edge and frisbee-shaped surrogate surfaces for making dry deposition measurements: Wind tunnel experiments and computational fluid dynamics (CFD) modeling

Jiaoyan Huang [a], Ying Liu [b], Thomas M. Holsen [a,b,*]

[a] Department of Civil and Environmental Engineering, Clarkson University, 8 Clarkson Ave., Potsdam, NY 13699-5712, USA
[b] Department of Environmental Science and Engineering, Clarkson University, 8 Clarkson Ave., Potsdam, NY 13699-5715, USA

ARTICLE INFO

Article history:
Received 11 January 2011
Received in revised form
28 April 2011
Accepted 3 May 2011

Keywords:
Surrogated surface
Knife-edge
Frisbee-shaped
Gas dry deposition
Wind tunnel

ABSTRACT

Dry deposition is a major pathway for atmospheric contaminant movement from the atmosphere to the earth surface. Despite its importance, there is no generally accepted direct method to measure dry deposition. Recently, the interest in using surrogate surfaces to measure dry deposition is growing, primarily because of their ease of use. However, a problem with these surfaces is extrapolating the results obtained to natural surfaces. There are two popular surrogate plates used to measure dry deposition. One had a sharp leading edge (knife-edge) (KSS), and the other has a smooth-edge (frisbee-shaped) (FSS). In this study, the performances of these two surrogate surfaces to directly measure gas dry deposition were explored using wind tunnel experiments and two-dimensional (2D) computational fluid dynamic (CFD) models. Although the fluid fields above these two plates were different, both created laminar boundary layers (distance above the surface where the velocity gradient is constant) with a constant thickness after approximately five cm. In the wind tunnel, gaseous elemental mercury (GEM) deposition to gold-coated filters was used to measure deposition velocities (V_d) in part because for this combination deposition is air-side controlled. The GEM V_d to both surfaces increased with increasing wind speeds. Based on both measurements and CFD simulations, the V_ds to the FSS were approximately 30% higher and more variable than to the KSS when the wind flow was parallel to the surfaces. However, when the angle between the surfaces and the wind was varied the V_ds to the FSS were less dependent on the incident angle than to the KSS.

1. Introduction

Deposition is the major pathway for air contaminants, such as trace metals, nitrate, sulfate, and toxic pollutants, to move from the atmosphere to the earth surface (Buehler and Hites, 2002; Landis and Keeler, 2002; Rolfhus et al., 2003). Although in general it is thought that wet and dry deposition are equally important (Lyman et al., 2007; Sakata et al., 2008; Shahin et al., 2000), the majority of the previous work has been concentrated on wet deposition because it is much easier to measure than dry deposition. Lyman et al. (2007) reported that in an arid area 60–75% of the total Hg deposition was due to dry deposition based on surrogate surface and soil flux measurements coupled with measured wet deposition from the mercury deposition network. Sakata et al. (2008) found that trace metal dry deposition fluxes were 1–10 fold higher than wet deposition in Japan using precipitation and water surface dry deposition samplers. Further complicating dry deposition measurements is the fact that for semi-volatile species both gas and particle phase deposition can be important.

Although there is still no widely acceptable method to measure dry deposition, with the advent of faster equipment, there is a growing interest in the use of micrometeorological techniques. However, these techniques cannot be used for large particles, when upwind surfaces are non-uniform or under non-uniform turbulence conditions (Lyman et al., 2009). Surrogate surfaces are another approach used to measure dry deposition fluxes. However, the behaviors of particles and gases are different. Bounceoff and resuspension can be important for particles but would not be considered for gas dry deposition. For gas dry deposition, the momentum boundary layer is important as is the chemical concentration profile beneath the roughness height.

* Corresponding author. Department of Civil and Environmental Engineering, Clarkson University, 8 Clarkson Ave., Potsdam, NY 13699-5712, USA. Tel.: +1 315 268 3851; fax: +1 315 268 7985.
E-mail address: tholsen@clarkson.edu (T.M. Holsen).

1352-2310/$ – see front matter © 2011 Elsevier Ltd. All rights reserved.
doi:10.1016/j.atmosenv.2011.05.013

Generally, surrogate surfaces are designed to minimize the turbulence on the surface and, therefore, provide a measure of the lower limit of dry deposition flux (Shahin et al., 2000). There are two different geometries commonly used, a knife-edge surrogate surface (KSS) and a frisbee-shaped surrogate surface (FSS). Both are symmetric plates and can create well-controlled boundary layers (distance above the surface where the velocity gradient is constant). The KSS has been widely used in field measurements since the1980s (Franz et al., 1998; Holsen et al., 1991; Lai et al., 2010; McCready, 1986; Noll et al., 1988; Shahin et al., 2000). The FSS was designed by Davidson et al. (1990) and was modified and tested in a wind tunnel by Wu et al. (1992b). The FSS has been used in the field since 1990 to measure the dry deposition fluxes of sulfate, nitrate, trace metals, SO_2, O_3, and gaseous oxidized mercury (GOM) (Landis and Keeler, 2002; Lyman et al., 2007; Marsik et al., 2007; Wu et al., 1992a; Zufall et al., 1998).

Based on boundary layer theory, the laminar boundary layer begins to develop at the front edge of the plate, and grows until its thickness becomes approximately constant. Wu et al. (1992a) reported that the FSS boundary layer thickness was constant after 10 cm from the leading edge. Assuming no surface resistance, the deposition velocity (V_d) at any point on the surface can be calculated as:

$$V_d = \frac{D}{L} \quad (1)$$

where D is the diffusivity of the depositing species in air, and L is the boundary layer thickness. Since the boundary layer thickness changes with position, V_d does as well. Other factors can impact the boundary layer thickness (and therefore V_d), including the angle of the wind relative to the surrogate surface (this dependency is likely different depending on the geometry of the surrogate surface) and the nature of the surface. For example, if the deposition surface is a liquid, water-side resistance can influence the V_d or mass transfer coefficient (MTC) (Lai et al., 2010).

The KSS and FSS are two popular surrogate surfaces used to measure gas dry deposition (Lai et al., 2010; Lyman et al., 2007, 2009); however, how these two different surfaces compare and how to extrapolate surrogate surface data to natural surfaces is largely unknown. This study compares the performance of these two surface geometries in a wind tunnel under controlled conditions to investigate important factors influencing the quasi-laminar layer, such as wind speed and sampler orientation. In addition, computational fluid dynamic (CFD) models were used to simulate dry deposition to each surface. Various collection media affecting gas dry deposition measurements were also investigated. Because of the ease of measurements, gaseous elemental mercury (GEM) was used in this study as a tracer gas. GEM deposition to the gold surface was used to mimic a rapid surface reaction (no surface resistance, such as GOM and HNO_3 to water).

2. Materials and methods

2.1. Wind tunnel description

The aerosol wind tunnel is an open-loop, Eiffel-type tunnel and is part of the Center for Air Resources Engineering and Science (CARES) facility. Air entering the tunnel passes through 21.2 m^2 of HEPA filters to remove ambient particles. Downstream from the filters are flow straightness and a 9:1 contraction to a cross-section 1.2 m wide by 0.9 m high. The tunnel can produce wind speeds of less than ~0.5 m s^{-1} to greater than 18 m s^{-1}. Exhaust was recirculated in the lab during the experiments to help maintain constant temperatures (20–23 °C) and humidity.

2.2. Sampling methods

2.2.1. Ambient air GEM concentrations

There are three species of mercury in air, GEM, GOM, and particulate-bounced mercury (PBM) (Schroeder and Munthe, 1998). In these experiments any PBM was removed as the air entered the tunnel. Since indoor GOM concentrations are very low (and any GOM that did exist was likely removed from the air as it passed through the HEPA filters); only GEM was assumed to be responsible for the measured deposition. The GEM concentration was measured at 5 min intervals in the air near the surrogate surface using PTFE tubing connected to a Tekran 2537A (Tekran, Inc., Toronto, Ontario, Canada) (flow rate 1 Lpm). The Tekran instrument analyzes total gaseous mercury in the air using two ultra-pure gold cartridges to trap vapor-phase mercury. Each cartridge is alternatively sampled and desorbed by heating and flushing with the carrier gas (argon). The desorbed mercury is quantified by cold-vapor atomic fluorescence (Tekran, 2001). The GEM concentrations were always above the published detection limits (0.1 ng m^{-3}) (Poissant et al., 2004). Internal calibration was performed daily.

2.2.2. GEM dry deposition fluxes

Three types of surrogate surfaces were used in this study (Fig. 1). The KSS was made from Teflon and has a sharp leading edge (around 10°). Lai et al. (2010) used a similar plate (40 cm diameter, 4 cm thickness) to measure speciated mercury dry deposition fluxes in Potsdam, NY. The influence of position on dry deposition velocity was tested using a rectangular KSS (Fig. 1a) using four filters placed in series. The Teflon FSS was designed by Keeler and Dvonch (2005) based on a design of Davidson et al. (1990) and has been used in previous studies to directly measure GOM dry deposition. For easy comparison, the KSS was the same size as the FSS (30 cm). Both surfaces had four circular indentations near their centers. During sampling, filter holders containing the sampling media were placed into the indentations which were designed so that the surface of the sampling media was at the same level as the top of the surrogate surface. The KSS and FSS were supported by tripods and placed in the wind tunnel to measure the GEM dry deposition fluxes. All surfaces were exposed facing up.

Two types of media were used in this study, gold-coated quartz fiber filters (GcQFF) and a 0.5% acidified BrCl solution (BrCl). Both of these media have large capacities and high efficiency in capturing GEM (Fialkowski et al., 2004; Lai et al., 2010). Gold was coated onto 47 mm quartz fiber filters (Whatman, Maidstone, Kent, UK) for 2 min using a Hummer VI-A sputter coater (Anatech Ltd., Union City, CA). Before sampling, they were cleaned by pre-heating at 550 °C in a mercury analytical system (Lai et al., 2010), placed into new plastic Petri dishes which were sealed with Teflon tape and parafilm, placed in double ziplock bags, and stored in the freezer. For field blanks, GcQFFs were placed in the tunnel on the samplers, briefly exposing them to ambient air, and subsequently treated the same as regular samples.

Saturated BrCl solution was premade in a particle free lab (240 mL 68% HCl + 60 mL MilliQ water + 3.30 g KBr + 4.50 g $KBrO_3$), stored in a Teflon bottle inside double ziplock bags, and placed in a refrigerator until use. For experiments, 200 mL of MilliQ water and 1000 μL saturated BrCl was placed into a cleaned Petri dish (15 cm width and 1.2 cm deep) located in the center of a KSS/FSS designed to keep the water surface level with the sampler surface. Fifty mL of this solution was then removed from the Petri dish using a pipette with a disposable tip and placed into a new plastic vial that was double zipper bagged as a field blank. The same amount of MilliQ water and 250 μL saturated BrCl were added back

into the Petri dish. All Teflon bottles and Petri dishes were cleaned following EPA method 1631E.

2.2.3. Analytical methods

The amount of Hg deposited onto the GcQFFs was determined using a thermal desorption system (Lai et al., 2010; Liu, 2008) made up of a quartz chamber surrounded by a ceramic heater. A zero air filter and Tekran 2537A analyzer were connected upstream and downstream, respectively. The quartz chamber can be heated up to 800 °C, and contains quartz chips and glass wool to ensure conversion of the desorbed Hg to GEM which was then transported to the analyzer with zero air for quantification. An injection port upstream of the chamber was used to check for leaks and determine recovery efficiencies.

For analysis, the GcQFF samples were placed into the chamber and the cool chamber (<50 °C) was flushed with zero air for two Tekran analysis cycles (5 min each). If the concentration was <0.5 ng m^{-3} for both cycles, the heater was turned on to release Hg

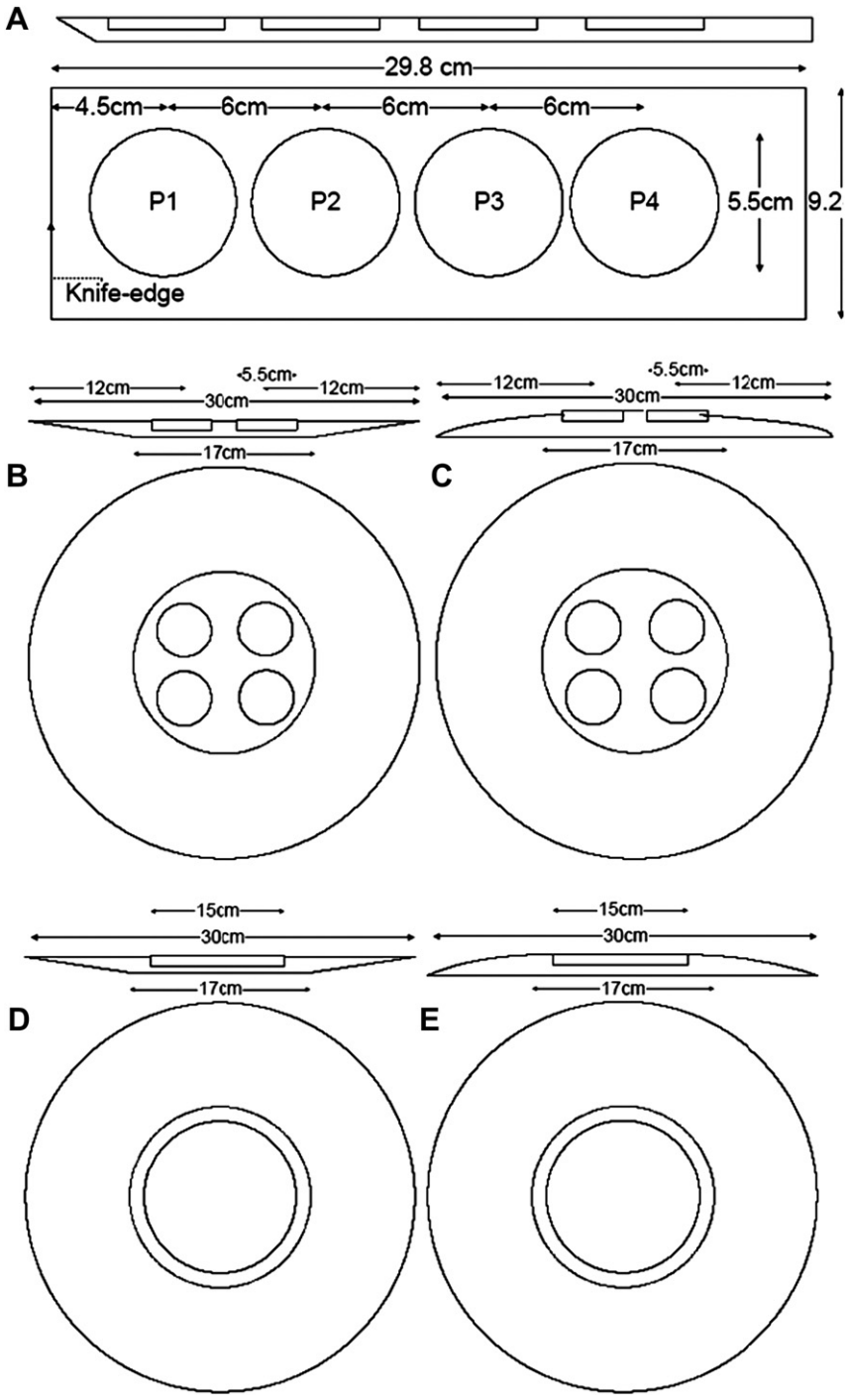

Fig. 1. Configuration of Knife-edge surrogate surface (KSS) and Frisbee surrogate surface (FSS), A) KSS with multiple filters to determine the influence of position on deposition velocity, B) KSS typically used in the field C) FSS, D) KSS with aqueous surface which is usually used in the field to measure deposition flux, E) FSS with aqueous surface which is usually used in the field to measure deposition flux.

from the filter. The heater was turned off when the concentration was again <0.5 ng m^{-3}. The mass of desorbed GEM was calculated using the measured concentration and flow rate. All aqueous samples were treated with 0.2% (v/v) $NH_2OH{\cdot}HCl$ to release halogens and analyzed using a Tekran 2600 following EPA method 1631E.

The recovery of GEM injections (using a Tekran 2505), standard reference material (SRM) 1633b (National Institute of Standards and Technology (NIST)), Hg^{2+} (15 ppb, diluted from SRM 1641d (NIST)) using the thermal desorption system were 93.1 ± 0.3, 85.6 ± 12.4, 95.0 ± 6.0%, respectively. The recoveries using the Tekran 2600 ranged from 80 to 120%. GcQFFs and BrCl blanks averaged 0.10 ± 0.08 ng for a blank filter ($n = 22$) and 0.55 ± 1.45 ng for a 200 mL solution ($n = 18$). The Hg mass associated with each blank was <10% of the Hg mass in a typical sample.

2.2.4. Computational fluid dynamics (CFD) methods

The CFD software FLUENT version 6.2 (Fluent Inc., Lebanon, NH) was used to solve for the flow fields around each the sampler. Geometries (2D) and their meshes were created using Gambit version 2.4.6 (Fluent Inc., Lebanon, NH). The modeled geometries closely replicated the actual sampler configuration. Grid insensitivity was confirmed by increasing the number of grids near the surface and rerunning the simulations. Both the laminar and shear-stress transport (SST) k–ω (turbulent) models were used. Convergences for simulations were $<1 \times 10^{-6}$; exact convergence values are included, along with other relevant FLUENT input parameters in the Supporting information (SI Table-1).

The species transport model was used in the CFD simulations to determine the GEM V_d. Although the deposition rate should be independent of ambient air concentration, the mass fraction of GEM was set as 1.63×10^{-12} kg kg^{-1}-air (2 ng m^{-3}) in the upwind air to mimic the Hg concentrations in the atmosphere (background GEM concentrations were approximately 1.7 ng m^{-3} (Slemr et al., 2003)). Species mass diffusivity was assumed to be 1.4×10^{-5} m^2 s^{-1} for GEM at 20 °C (Massman, 1999).

2.2.5. Deposition velocity and mass transfer coefficient calculation

Experimental V_ds (or MTCs) were determined using:

$$F = \frac{M_{Hg}}{A \times T_{exp}} = D_A \frac{C_A - C_S}{L} = (V_d \text{ or MTC}) \times C_A \quad (2)$$

where M_{Hg}, A, T_{exp}, D_A, C_A, C_s, and L are Hg mass on a filter or in the solution, the collecting surface area, exposure time, GEM diffusivity in air, GEM concentration in the bulk air, GEM air concentration on the collecting surface, and boundary layer thickness, respectively. Since the GcQFF was considered to be a perfect sink for GEM, C_s was assumed to be zero. For calculations based on the Blasius's solution L was the thickness of the layer for which the velocity was linearly correlated with distance from surface. In CFD simulations, the concentration gradient was calculated using the first grid values after it was verified that the simulated gradient was liner in this region ($V_d = D_A \times \frac{dC}{dL}/C_A$).

3. Results and discussions

3.1. The influence of position on V_d to the KSS

Based on Blasius's solution for the laminar boundary layer over a flat plate (Welty et al., 2001), the V_d should be proportional to $\sqrt{U/x}$ where U is the bulk wind velocity and x is the distance from the leading edge. In wind tunnel experiments using the KSS (performed in triplicate) at wind speeds of 2, 3, and 5 m s^{-1} V_d was found to increase with increasing wind speed and decrease with increasing distance consistent with laminar boundary layer theory (Fig. 2). Theoretical V_d values compared well with CFD simulated values (laminar model) with relative percent differences (RPD, $RPD = 100 \times |A - P|/A$, where P and A are predicted and measured values, respectively) of 7.5 ± 3.1, 9.8 ± 3.5, and 12.7 ± 6.6% for 2 m s^{-1}, 3 m s^{-1} and 5 m s^{-1}, respectively. RPDs generally decreased with increasing distance from the leading edge and were similar at all wind speeds (at 3 m s^{-1} wind speed RPDs were 14, 12, 6, and 8%, respectively).

The CFD laminar model simulations were 49 ± 2, 42 ± 6, and 54 ± 2% lower than the measured values, for 2 m s^{-1}, 3 m s^{-1}, and 5 m s^{-1}, respectively (Fig. 2) and generally agreed better farther from the leading edge. This difference between measured and modeling results is probably because there is some turbulence in the tunnel. The K-omega shear-stress transport (SST) model is usually applied to explore the flow close to a wall. Assuming 2% turbulence best matched the measured results (RPDs at 2, 3, and 5 m s^{-1} were 37 ± 12, 9 ± 11, and 11 ± 11%, respectively). (Hereafter, presented CFD simulations were from the k-omega SST 2% turbulent model.)

Based on the experimental measurements, CFD simulations, and theoretical calculations, the boundary layer thickness was still changing significantly up to 5 cm from leading edge at all wind speeds. After 5 cm, the boundary layer thickness was relatively constant. Experimental measurements of V_d for the first position were more variable than for the other three positions (larger error bars) and the difference between measurements and predicted values was the greatest (average RPDs at different positions were 33, 17, 15, and 9%, starting from first position). The deposition

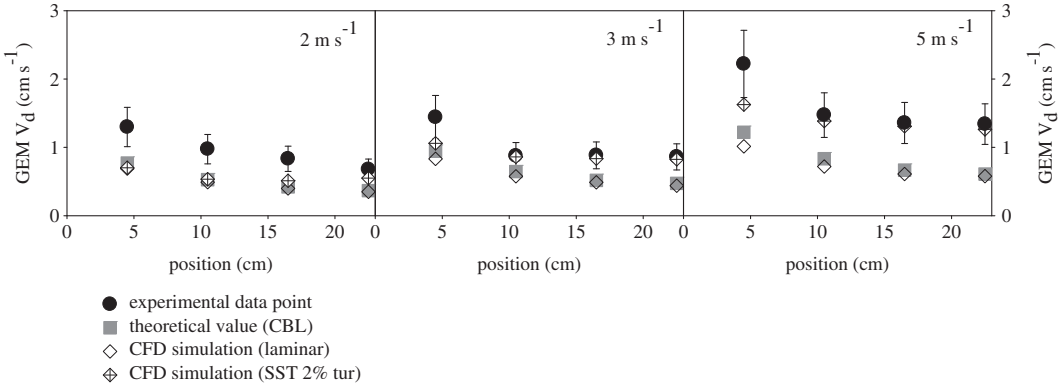

Fig. 2. GEM dry deposition velocities as a function of position and wind speed measured in wind tunnel experiments, simulated using CFD, and calculated using laminar boundary theory on a flat plate.

velocity at the first position and other three positions were statistically different (*t*-test, $p < 0.001$). In particular at low wind speed (2 m s^{-1}), the CFD simulation underestimated the measured V_d; however, at higher wind speeds the V_ds from simulations and measurements were in good agreement (averaged RPD at 3 and 5 m s^{-1}at the first position was 26% and at the other position was 4.5%).

3.2. Comparison between KSS and FSS

To determine how the shape of the surrogate surface impacts measured V_ds, the KSS and FSS were tested with four GcQFFs in triplicate in the wind tunnel at various wind speeds (2, 3, 5 m s^{-1}) and angles with respect to the wind. In addition, CFD modeling was used to determine the fluid field near the plates. V_ds were statistically different (*t*-test, $p < 0.001$) at different wind speed and orientations. In general, for a horizontal orientation the V_d to the FSS was 30% larger than to the KSS, because the front edge of the FSS created turbulent eddies that interacted with the boundary layer causing it to be thinner. Over the KSS; however, the boundary layer developed smoothly from the front edge (Fig. SI1) and in a shorter distance than for the FSS. Overall, both plates created a well-controlled laminar layer near the center of the plates.

It was hard to determine the exact boundary layer thickness in these simulations; however, the velocity gradient over the FSS center (15 cm from edge) was 30% greater than over the KSS center. This indicates that the velocity profile changed more rapidly over the FSS than over the KSS. This rapid change resulted in a smaller boundary layer thickness and larger V_ds. For these experiments, four GcQFFs were placed near the center of the samplers. Simulations suggested that all of the positions should measure similar deposition velocities. Higher V_d standard deviations were measured for the FSS than for the KSS (Fig. 3 top), probably because higher turbulent intensity was observed over the FSS (10–30%) than over the KSS (10–15%), especially near the front edge (Fig. SI2). These eddies cause the flow to be unsteady and explain the large standard deviations and larger difference between measured and modeled V_d for the FSS than for the KSS.

For both surfaces, V_d was found to increase with increasing wind speed (Fig. 3 top). The difference between measured and simulated values ranged from −15 to 28%. In Potsdam, NY and Reno, NV the measured V_d of GEM to a KSS and RGM to an FSS was ~0.7 and ~1 cm s^{-1} respectively (Lai et al., 2010; Lyman et al., 2007). Using a typical wind velocity of 2 m s^{-1} the GEM V_d converted from GOM using a diffusivity of 1.0 cm^2 s^{-1} was 1.3 cm s^{-1} which is similar to the wind tunnel results reported here.

Another important factor affecting the deposition velocity is the angle of the surrogate surface with respect to the wind. Wind generally flows parallel with the ground surface under the planetary boundary layer; however, microenvironments such as forests, buildings, and hills can create vertical wind vectors. These vectors produce altered fluid flow near the collection surface and may influence V_ds (or MTCs). This potential impact was investigated by placing the surfaces at two different angles (15° facing the wind and 15° against the wind) at 3 m s^{-1} wind speed. Based on FLUENT simulations (Fig. 3 bottom), the V_ds to the FSS ranged between 1.0 and 1.3 cm s^{-1} (lowest at +15° and highest at −15°) and were more constant than for the KSS which ranged between 0.73 and 1.71 cm s^{-1} (lowest in 0° and highest in +15°) (Fig. 3) (Fig. 3 bottom). The RPD between the V_ds to the KSS predicted from FLUENT and measured in experiments range from 8 to 25% and were lower than for the FSS (range from 27 to 56%). Similar to the horizontal results the standard deviation of the V_ds was higher for the FSS than for the KSS.

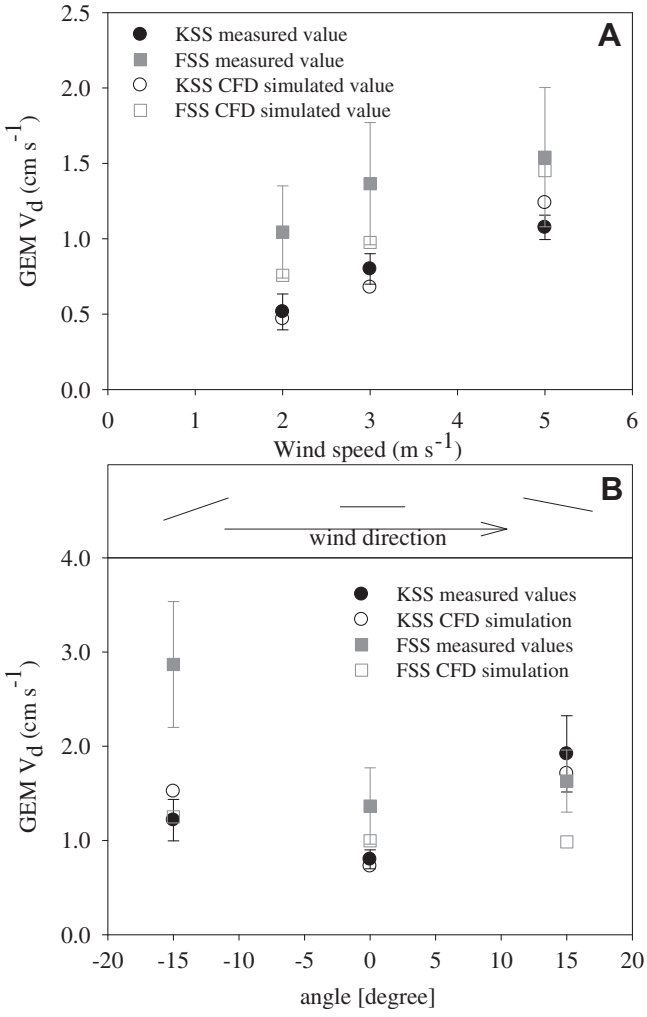

Fig. 3. Comparison of GEM dry deposition velocities measured in the wind tunnel and simulated using FLUENT for both the KSS and FSS surrogate surfaces A) different wind speeds and B) different angles.

3.3. Comparison between BrCl and GcQFFs

Lai et al. (2010) reported that GcQFFs had larger deposition velocities for GEM than BrCl when used as the collection media on

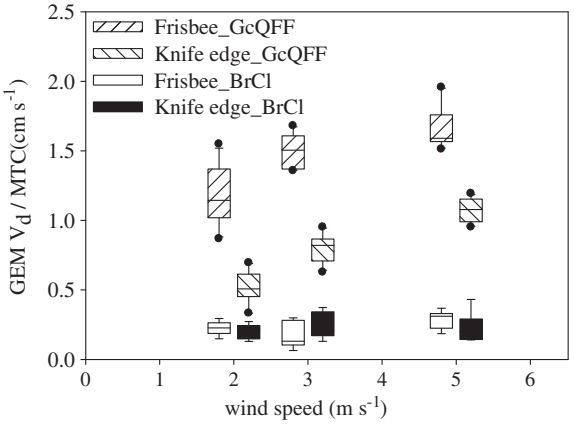

Fig. 4. Comparison between the measured GEM dry deposition velocities to acidified BrCl solutions and to GcQFF in the wind tunnel for both the KSS and FSS.

a KSS. The same findings were observed in this study (Fig. 4). The V_ds to the GcQFF were 3–8 times higher than MTCs to BrCl solutions. The MTCs were consistent regardless of wind speed and plate shape, which implies that for the BrCl solution deposition was controlled by water-side resistance (air-side boundary layer resistance was negligible).

For a solid collecting surface with very fast reaction, such as GcQFFs, the air boundary controls deposition. However, if the collection surface is an aqueous solution the water-side boundary layer can provide additional resistance. The flux using two-film theory is represented by Eqs. 3 and 4, the product of the MTC (K_{AW}) and the fugacity difference. The overall MTC (K_{AW}) across both the air and liquid boundary layer can be expressed as:

$$\text{Flux} = K_{AW}(c_a - H_{cc}C_W) \tag{3}$$

$$K_{AW} = \frac{1}{\frac{1}{k_A} + \frac{H}{k_W}} \tag{4}$$

where k_A, k_W, and H are the air-side MTC, water-side MTC and Henry's law constant, respectively. Because of the low solubility of GEM (Lai et al., 2007), $H_{cc}C_w$ is small. k_A can be determined from the solid surrogate surface (GcQFF) experiments (assuming the amalgamation reaction is very fast) and K_{AW} can be determined from the aqueous surface experiments. Assuming relatively fast reactions occurred in the water-side boundary converting the GEM to Hg^{2+} k_w is (Cussler, 1997):

$$k_W = \sqrt{D_W\kappa} \text{ or } \kappa = k_W^2 D_W \tag{5}$$

where D_W and κ are the diffusivity of GEM in water (1.5×10^{-5} cm^2 s^{-1}) and the reaction rate constant (Kuss et al., 2009). Assuming this reaction can be described as (Lindberg et al., 2002):

$$\begin{aligned} &Hg^0_{(aq)} + BrCl_{(aq)} \leftrightarrow Hg^{2+}_{(aq)} \\ \text{Rate} &= k_1\left[BrCl_{(aq)}\right]\left[Hg^0_{(aq)}\right] = k\left[Hg^0_{(aq)}\right] \end{aligned} \tag{6}$$

the pseudo-first order reaction rate constant determined assuming $[BrCl_{(aq)}]$ was constant (9.32×10^{-4} M) is 6.7 ± 2.3 $\times 10^5$ M^{-1} s^{-1}. Although no value for this rate constant (elemental mercury with BrCl in aqueous) was found, $\kappa_1$of elemental mercury reacting with O_3, OH, Cl_2, Br_2 (at pH = 2), HOBr (at pH = 6.8), and OBr^- (at pH = 11.7) were ~5×10^7, 2×10^9, 2×10^6, 0.20, 0.28, and 0.27 M^{-1} s^{-1}, respectively (Lin and Pehkonen, 1999; Wang and Pehkonen, 2004).

4. Conclusions

Wind tunnel experiments and CFD simulations were used to compare performances of two surrogate surfaces. Both the KSS and FSS were found to create a well-controlled laminar boundary layer near their centers based on CFD results. The boundary layer had a relatively constant thickness after approximately 5 cm from the edge. V_d was approximately 30% higher to the FSS than to the KSS, because the boundary layer was thinner due to turbulent eddies caused by the blunt leading edge of the FSS which interacted with the boundary layer. These eddies also likely caused the greater variability in V_ds measured in the central region of the FSS than in the central region of the KSS. Potential advantages of the FSS over the KSS were that the V_ds were more independent of the angle between the surface and the wind for the FSS than for the KSS. Flow is generally assumed to be parallel with a surrogate surface. However recently, Lyman et al. (2007) measured two to five fold higher dry deposition velocities of GOM to surrogate surfaces than estimated using the multiple resistance model. This difference might be due in part to the sampler orientation relative to the flow field. Experiments with GcQFF and acidified BrCl solutions found higher V_ds to the GcQFF than to the BrCl probably because of increased resistance in the aqueous phase due to slower reaction rates. The results indicate both plates can be applied in the field to examine dry deposition.

Acknowledgments

The authors are grateful to Frank Marsik and Gerald Keeler at the University of Michigan for loaning us an FSS. In addition, we would like to acknowledge Suresh Dhaniyala, Samring Lee, Douglas Leonard, Andy May, and Arash Moharreri from Clarkson University for assistance in performing CFD simulations and wind tunnel experiments. This work was funded in part by the Great Lakes Commission through a Great Lakes Atmospheric Deposition Grant (Jon Dettling Project Officer).

Appendix. Supporting information

Supporting information related to this article can be found online at doi:10.1016/j.atmosenv.2011.05.013.

References

Buehler, S.S., Hites, R.A., 2002. Peer reviewed: the great lakes' integrated atmospheric deposition network. Environmental Science & Technology 36, 354A–359A.
Cussler, E.L., 1997. Diffusion-mass Transfer in Fluid Systems. The Press Sydicate of the University of Cambridge, Cambridge, MA.
Davidson, C.I., McRae, G.J., Gamble, J.S., 1990. Detector for dry deposition of atmospheric contaminants having a coating capable of retaining contaminants, In: Patent, U.S. (Ed.).
Fialkowski, M., Grzeszczak, P., Nowakowski, R., Holyst, R., 2004. Absorption of mercury in gold films and its further desorption: quantitative morphological study of the surface patterns. The Journal of Physical Chemistry B 108, 5026–5030.
Franz, T.P., Eisenreich, S.J., Holsen, T.M., 1998. Dry deposition of particulate polychlorinated biphenyls and polycyclic aromatic hydrocarbons to Lake Michigan. Environmental Science & Technology 32, 3681–3688.
Holsen, T.M., Noll, K.E., Liu, S.P., Lee, W.J., 1991. Dry deposition of polychlorinated biphenyls in urban areas. Environmental Science & Technology 25, 1075–1081.
Keeler, G.J., Dvonch, J.T., 2005. Atmospheric mercury: a decade of observations in the great lakes. In: Pirrone, N., Mahaffey, K.R. (Eds.), Dynamics of Mercury Pollution on Regional and Global Scales: Atmospheric Processes and Human Exposures Around the World. Springer Publishers, Norwell, MA, pp. 611–636.
Kuss, J., Holzmann, J.r., Ludwig, R., 2009. An elemental mercury diffusion coefficient for natural waters determined by molecular dynamics simulation. Environmental Science & Technology 43, 3183–3186.
Lai, S.-O., Holsen, T.M., Han, Y.-J., Hopke, P.P., Yi, S.-M., Blanchard, P., Pagano, J.J., Milligan, M., 2007. Estimation of mercury loadings to Lake Ontario: results from the Lake Ontario atmospheric deposition study (LOADS). Atmospheric Environment 41, 8205–8218.
Lai, S.-O., Huang, J., Hopke, P.K., Holsen, T.M., 2010. An evaluation of direct measurement techniques for mercury dry deposition. Science of the Total Environment 409, 1320–1327.
Landis, M.S., Keeler, G.J., 2002. Atmospheric mercury deposition to Lake Michigan during the lake Michigan mass balance study. Environmental Science & Technology 36, 4518–4524.
Lin, C.-J., Pehkonen, S.O., 1999. The chemistry of atmospheric mercury: a review. Atmospheric Environment 33, 2067–2079.
Lindberg, S.E., Brooks, S., Lin, C.J., Scott, K.J., Landis, M.S., Stevens, R.K., Goodsite, M., Richter, A., 2002. Dynamic oxidation of gaseous mercury in the Arctic troposphere at polar sunrise. Environmental Science & Technology 36, 1245–1256.
Liu, Y., 2008. Analysis Method and Direct Measurement Technologies for Mercury Dry Deposition. Department of Environmental Science and Engineering, Clarkson Univeristy, Potsdam.
Lyman, S.N., Gustin, M.S., Prestbo, E.M., Marsik, F.J., 2007. Estimation of dry deposition of atmospheric mercury in Nevada by direct and indirect methods. Environmental Science & Technology 41, 1970–1976.
Lyman, S.N., Gustin, M.S., Prestbo, E.M., Kilner, P.I., Edgerton, E., Hartsell, B., 2009. Testing and application of surrogate surfaces for understanding potential gaseous oxidized mercury dry deposition. Environmental Science & Technology 43, 6235–6241.

Marsik, F.J., Keeler, G.J., Landis, M.S., 2007. The dry-deposition of speciated mercury to the Florida Everglades: measurements and modeling. Atmospheric Environment 41, 136–149.
Massman, W.J., 1999. Molecular diffusivities of Hg vapor in air, O_2 and N_2 near STP and the kinematic viscosity and thermal diffusivity of air near STP. Atmospheric Environment 33, 453–457.
McCready, D.I., 1986. Wind tunnel modeling of small particle deposition. Aerosol Science and Technology 5, 301–312.
Noll, E.K., Fang, K.Y.P., Watkins, L.A., 1988. Characterization of the deposition of particles from the atmosphere to a flat plate. Atmospheric Environment 22, 1461–1468.
Poissant, L., Pilote, M., Constant, P., Beauvais, C., Zhang, H.H., Xu, X., 2004. Mercury gas exchanges over selected bare soil and flooded sites in the bay St. François wetlands (Québec, Canada). Atmospheric Environment 38, 4205–4214.
Rolfhus, K.R., Sakamoto, H.E., Cleckner, L.B., Stoor, R.W., Babiarz, C.L., Back, R.C., Manolopoulos, H., Hurley, J.P., 2003. Distribution and fluxes of total and methylmercury in Lake Superior. Environmental Science & Technology 37, 865–872.
Sakata, M., Tani, Y., Takagi, T., 2008. Wet and dry deposition fluxes of trace elements in Tokyo Bay. Atmospheric Environment 42, 5913–5922.
Schroeder, W.H., Munthe, J., 1998. Atmospheric mercury – an overview. Atmospheric Environment 32, 809–822.
Shahin, U., Yi, S.-M., Paode, R.D., Holsen, T.M., 2000. Long-term elemental dry deposition fluxes measured around Lake Michigan with an automated dry deposition sampler. Environmental Science & Technology 34, 1887–1892.
Slemr, F., Brunke, E.G., Ebinghaus, R., Temme, C., Munthe, J., Wangberg, I., Schroeder, W., Steffen, A., Berg, T., 2003. Worldwide trend of atmospheric mercury since 1977. Geophysical Research Letters 30 Art. No. 1516.
Tekran, 2001. Tekran Model 1130 Mercury Speciation Unit and Model 1135-p Particulate Mercury Unit Toronto, Canada.
Wang, Z., Pehkonen, S.O.S.O., 2004. Oxidation of elemental mercury by aqueous bromine: atmospheric implications. Atmospheric Environment 38, 3675–3688.
Welty, J.R., Wicks, C.E., Wilson, R.E., Rorrer, G., 2001. Fundamentals of Momentum, Heat, and Mass Transfer. John Wiley & Sons, Hobeken, NJ.
Wu, Y.-L., Davidson, C.I., Dolske, D.A., Sherwood, S.I., 1992a. Dry deposition of atmospheric contaminants: the relative importance of aerodynamic, boundary layer, and surface resistances. Aerosol Science and Technology 16, 65–81.
Wu, Y.-L., Davidson, C.I., Russell, A.G., 1992b. Controlled wind tunnel experiments for particle bounceoff and resuspension. Aerosol Science and Technology 17, 245–262.
Zufall, M.J., Davidson, C.I., Caffrey, P.F., Ondov, J.M., 1998. Airborne concentrations and dry deposition fluxes of particulate species to surrogate surfaces deployed in southern Lake Michigan. Environmental Science & Technology 32, 1623–1628.